Available online at www.sciencedirect.com
ScienceDirect
Journal of Power Sources 170 (2007) 251–258
JOURNAL OF POWER SOURCES
www.elsevier.com/locate/jpowsour

Methane-fueled IT-SOFCs with facile in situ inorganic templating synthesized mesoporous $Sm_{0.2}Ce_{0.8}O_{1.9}$ as catalytic layer

Kang Wang, Ran Ran, Zongping Shao *

College of Chemistry and Chemical Engineering, Nanjing University of Technology, No. 5 Xin Mofan Road, Nanjing 210009, JiangSu, PR China

Received 19 January 2007; received in revised form 10 April 2007; accepted 17 April 2007
Available online 22 April 2007

Abstract

Mesoporous $Ce_{0.8}Sm_{0.2}O_{1.9}$ (SDC) oxide with high surface area was prepared by a novel glycine-nitrate combustion process with in situ created nickel oxide as template, and applied as the catalytic layer for methane-fueled solid-oxide fuel cells (SOFCs) operated at reduced temperatures. The weight ratio of nickel oxide to SDC in the synthesis process was found to have significant effect on both the crystallite size and the textural properties of the resulted SDC powder. In particular, when it was at 9, the thermally stable and well-crystallized SDC powder showed a mesoporous structure with narrow pore-size distribution, high surface area (77 $m^2\ g^{-1}$) and large pore volume (~0.2276 $cm^3\ g^{-1}$), even after the calcination at 700 °C for 3 h. The mesoporous SDC was found to favor free gas diffusion with no gas diffusion polarization occurred even at high current density both for hydrogen and methane fuels. The SOFC with Ru impregnated mesoporous SDC catalytic layer displayed promising performance with a peak power density of ~462 mW cm^{-2} at 650 °C.

Keywords: Doped ceria; Mesoporous; Methane; Catalyst; Solid-oxide fuel cells

1. Introduction

Fuel cells are attractive power-generation technologies that directly and efficiently convert chemical energy to electrical power via the silent and environmental friendly electrochemical way. For most of the fuel cells, high-purity hydrogen is usually required as the fuel. However, due to the lack of public hydrogen production, storage and transportation infrastructure, the wide spread of hydrogen fuel cell may not be so optimistic within the next few decades. The much more matured infrastructure of gasoline and home gas system makes the hydrocarbon fuel cell more realistic in the near future. Solid-oxide fuel cells (SOFCs) are such kind of fuel cells that can operate directly with hydrocarbon fuel without the need of external reforming process. However, because of the less electrochemical activity of hydrocarbon than hydrogen over the typical nickel-based anode, a better performance electrochemical catalyst for hydrocarbon oxidation is necessary for practical application purpose. Ceria oxide has been found to be an excellent high-active catalyst for hydrocarbon oxidation and cracking [1–5]. Electrochemical oxidation of hydrocarbons using ceria-based anode has also been successfully reported [6–9]. For example, it demonstrated that the addition of CeO_2 to the anode of Cu–Yttria stabilized zirconia/SDC cermets significantly enhanced the cell performance with hydrocarbon fuels [6].

Recently it was recognized that the ceria in mesoporous state could greatly improve the catalytic activity for hydrocarbon oxidation as compared to the bulk ceria [10–12]. Nonperiodic hierarchical mesoporosity coupled with nanocrystallinity has the potential to enhance mass transport, ionic and electronic mobility, and in particular maximize the three-phase-boundary (TPB) length in cathode or anode [12]. Significant improvement of fuel cell performance by applying mesoporous ceria catalytic layer has been demonstrated [13,14].

Up to now, undoped ceria was mostly applied as the electrocatalyst in SOFCs. Due to the poor ionic conductivity (<10^{-4} S cm^{-1}), it mainly functioned as the reforming/oxidation catalyst with improved gas diffusion properties but negligible contribution to the extension of the TPB length. The doping of CeO_2 with Sm_2O_3 or Gd_2O_3 leads to the substantially increase of the ionic conductivity to a level of ~0.01 S cm^{-1} at 600 °C and ~0.1 S cm^{-1} at 800 °C. Therefore, an increase

* Corresponding author. Tel.: +86 25 83587722; fax: +86 25 83365813.
E-mail address: shaozp@njut.edu.cn (Z. Shao).

0378-7753/$ – see front matter © 2007 Elsevier B.V. All rights reserved.
doi:10.1016/j.jpowsour.2007.04.030

of the fuel cell performance is possible from the extension of the TPB length by applying the doped ceria as the catalyst. For example, it was reported that the coating of the pores of Ni/ScSZ (scandia-stabilized zirconia) anode with 2 wt.% nano-sized $Gd_{0.2}Ce_{0.8}O_{1.9}$ conducting particles yielded much higher power density than that without the ceria modification [13]. The combination of high ionic conductivity and mesoporosity of the doped ceria may result in the substantially increase of the fuel cell performance. Therefore, in this study we are aimed at the synthesis of mesoporous SDC and the application of it as the electrocatalyst for reduced temperature methane-fueled SOFCs.

In literature, several methods have been used for the preparation of mesoporous ceria powders [15–19]. In those methods, fine and mesoporous ceria powders were produced by applying relatively expensive surfactants and organic templates. Furthermore, the synthesized powders always showed poor thermal and mechanical stability, which greatly limited their application in SOFCs. Here, we reported an innovative in situ inorganic templating process for the facile synthesis of mesoporous nano-crystalline SDC power with high thermal stability. A glycine-nitrate combustion process (GNP) with in situ created nickel oxide as the agglomeration inhibitor and template was applied for the synthesis of mesoporous SDC powders. The method takes the advantages of cheap raw material, fast synthesis, recyclable inorganic template, high thermally stable and well-crystallized SDC. The as-prepared mesoporous SDC was loaded with Ru and applied as the catalytic layer for methane-fueled SOFCs operated at intermediate temperature with promising performance.

2. Experimental

2.1. Synthesis of SDC powder and fabrication of fuel cell MEA (Membrane-electrode-assembly) with catalyst layer

A modified glycine-nitrate process was applied for the synthesis of mesoporous SDC, which was schematically shown in Fig. 1. Stoichiometric amount of ceria nitrate ($Ce(NO_3)_3{\cdot}6H_2O$, >99%), samarium nitrate ($Sm(NO_3)_3{\cdot}6H_2O$, >99%) and nickel nitrate ($Ni(NO_3)_2{\cdot}6H_2O$, >99%), according to the aimed ratio, was prepared into a mixed aqueous solution in a Pyrex breaker. Glycine (NH_2–CH_2–COOH, 99%) was added to the mixed solution at the mole ratio of glycine:total metal ions at 2:1. The solution precursor was then heated at ~90 °C over a hot plate under vagarious magnetic stirring until a gel was obtained, which was then transferred to a heated oven at 250 °C for a self-sustaining combustion. After the reaction, the primary products were further calcined at 700 °C under stagnant air for 3 h at the heating/cooling rate of 5 °C min^{-1} to remove the carbon residues in the powders and form the well-crystallized powders. The as-obtained powders were then soaked with a 3 mol L^{-1} HNO_3 aqueous solution and heated at 90 °C for several hours under stirring. The nickel oxide in the powder was dissolved by the HNO_3 to leave a porous SDC powder, which was then filtered and washed with deionized water and ethanol. The obtained nickel nitrate solution can be recycled and applied as the raw material for the next synthesis.

The anode-supported cells with SDC as electrolyte were prepared by a dual dry-pressing process. Anode powder consisting

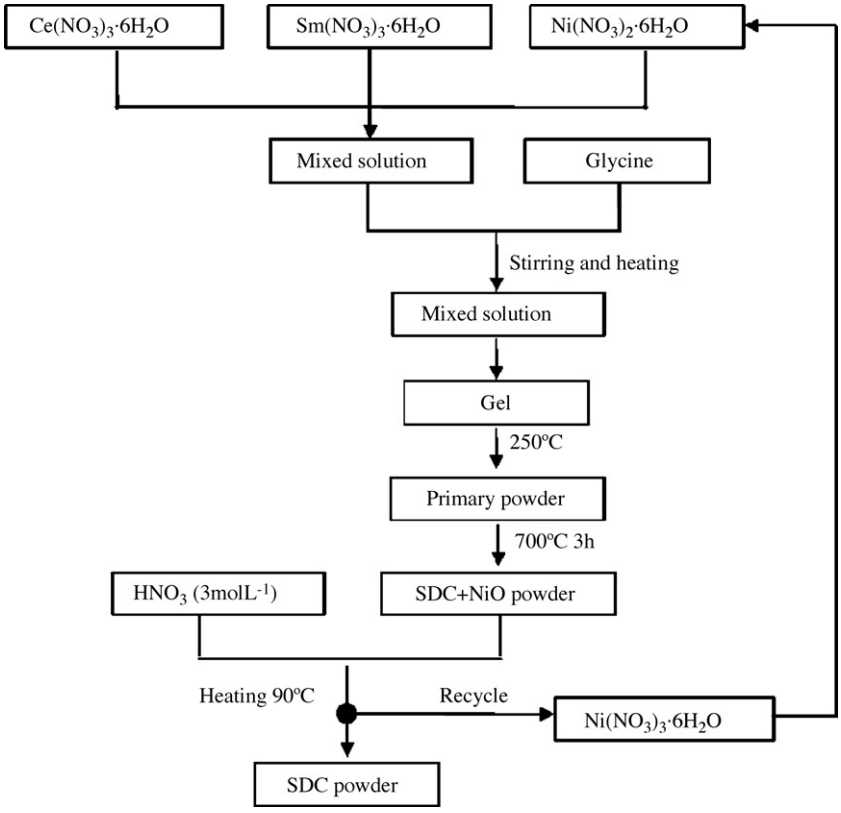

Fig. 1. Schematic diagram for the preparation of mesoporous SDC powder via the modified GNP method with in situ created NiO as template.

of 60 wt.% NiO and 40 wt.% SDC was prepared by high energy ball milling (FRITSCH, Pulverisette 6) of the mixture of NiO and SDC. To fabricate a single cell, NiO–SDC anode powder was firstly pressed as a substrate. SDC powder was added onto the substrate surface and pressed again to form a bi-layer pellet, which was then fired at 1350 °C to result in the densification of the electrolyte layer (area: ~1.25 cm^2). Slurry, consisting of $Ba_{0.5}Sr_{0.5}Co_{0.8}Fe_{0.2}O_{3-\delta}$ (BSCF) (synthesized by a combined EDTA–citrate complexing method [20]) + SDC (30 wt.% SDC), was applied to the electrolyte surface by painting method, which was subsequently calcined at 1000 °C under air atmosphere for 5 h to form a porous cathode layer (area: ~0.48 cm^2). For the single cell with the catalytic layer, slurry consisting of 7 wt.% Ru-loaded mesoporous SDC was applied onto the surface of NiO + SDC anode layer at 150 °C by screen painting method, followed by dried at 250 °C for 3 h and in situ calcined at 650 °C under hydrogen. The Ru-loaded SDC catalyst was prepared by the impregnation method. For a typical experiment, an appropriate amount of $RuCl_3$ and binder PVB was added to a suspension consisting of 0.5 g mesoporous SDC powder and 10 mL ethanol, followed by grinding for 30 min with an agate mortar and pestle and then well mixed by ultrasonic vibration for 1 h.

2.2. Characterization

The lattice structure of the synthesized powders was determined by X-ray diffraction (XRD, Bruker D8 Advance) using Cu Kα radiation (λ = 1.54056 Å). The experimental diffraction patterns were collected at room temperature by step scanning at the range of $10° \leq \theta \leq 90°$. The peak broadening effect was used to determine the average crystallite size according to the Scherrer equation. The N_2 adsorption measurement was performed using a BELSORP II instrument at the temperature of liquid nitrogen to determine the specific surface area, pore volume and pore-size distribution of the prepared powders. The specific surface area and the pore-size distribution were calculated based on the Brunauer–Emmett–Telley (BET) and Barrett–Joyner–Halenda (BJH) methods, respectively. Before the measurement, the samples were pre-treated at 100 °C for 3 h under vacuum to remove the surface–adsorbed species. The morphologies of the powders and the fuel cells were examined by an environmental scanning electron microscope (ESEM, Quanta-2000). The fuel cell performance was tested by I–V characterization using a digital sourcemeter (Keithley 2420) interfaced with computer for data acquisition. Three percentage of H_2O humidified H_2 or CH_4 was used as the fuel and ambient air as the cathode atmosphere during the fuel cell test.

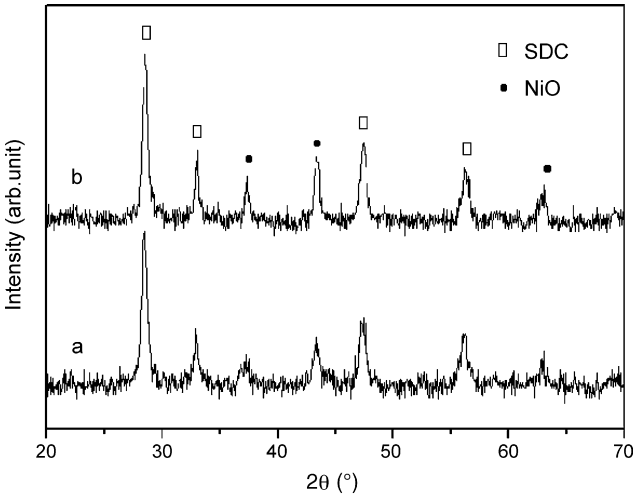

Fig. 2. X-ray diffraction pattern of the powder from the GNP process with nickel nitrate additive: (a) fresh combustion-synthesized powder and (b) the powder after further calcined at 700 °C for 3 h.

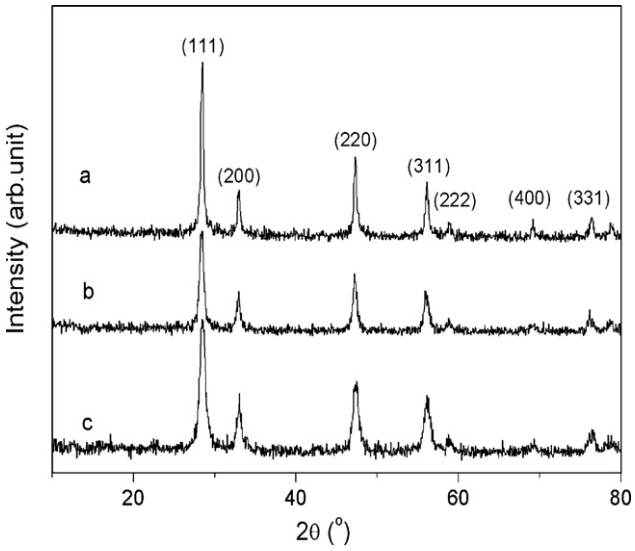

Fig. 3. X-ray diffraction patterns of SDC powders prepared from the NiO-templated GNP process at NiO/SDC weight ratio of (a) 0 (without NiO); (b) 1; (c) 9. The mirror index is based on the cubic phase of SDC.

3. Results and discussion

For the GNP combustion process, significant different combustion behaviors were observed with and without the presence of nickel nitrate in the precursor. It was volume combustion type for the case without the presence of nickel nitrate. The resulted powder took the color of light yellow. However, some black residual was also observed over the inner wall of the beaker, which suggests that the reaction was not completely finished. For the precursor with nickel nitrate, the combustion changed to a self-propagated type of reaction. It began along the inner wall of the beaker and propagated towards the middle. The resulted powder was very light in weight and took the morphological shape of branch and the color of gray. There was almost no residual observed over the wall of the beaker, suggesting the complete reaction of the materials. The reactions stopped in seconds for both cases. The phase purity and the lattice structure of the as-

Table 1
Effect of different weight ratios of NiO/SDC on the properties of SDC powder

Weight ratio	D_{XRD} (nm)	S_{BET} ($m^2\ g^{-1}$)	Pore volume ($cm^3\ g^{-1}$)
0	13.7	15	0.1165
1	9.3	49	0.2155
9	6.7	77	0.2276

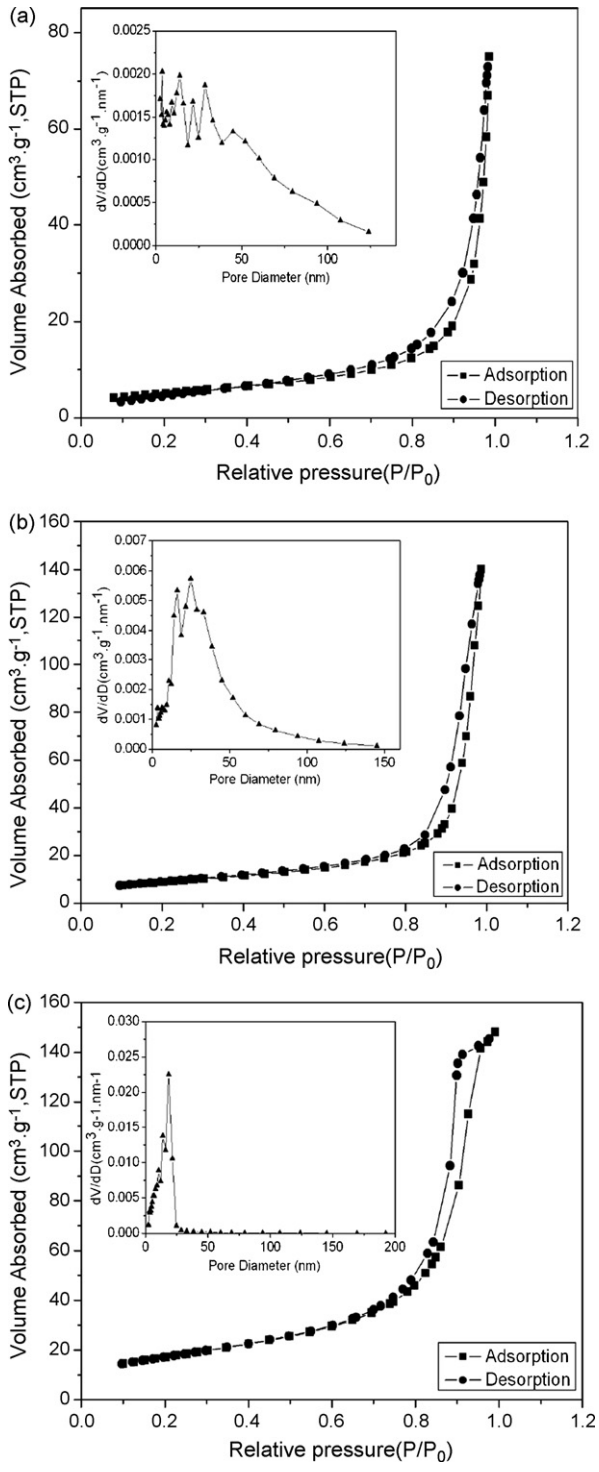

Fig. 4. Nitrogen adsorption–desorption isotherms patterns of as-synthesized SDC powders with NiO to SDC weight ratio of: (a) 0 (without NiO); (b) 1; (c) 9, the corresponding BJH pore-size distribution of the samples showed in the inset.

synthesized powders were then examined by X-ray diffraction (XRD). As shown in Fig. 2, it was established that the powders were composed of NiO and face-centered phase of SDC, both for the fresh combustion-synthesized powder and the powder after further calcination at 700 °C for 3 h. It suggests no phase reaction happened between nickel oxide and samaria oxide/ceria oxide.

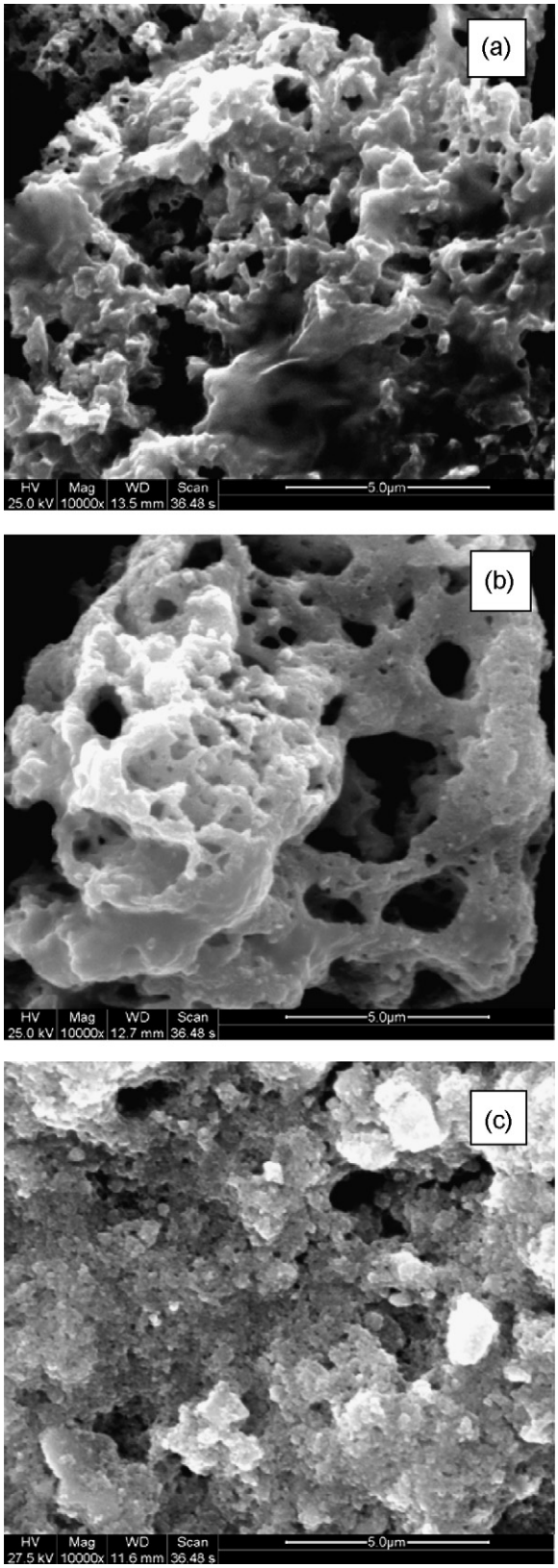

Fig. 5. SEM images of SDC powders prepared by the NiO-templated GNP process at NiO to SDC weight ratio of (a) 0 (without NiO); (b) 1; (c) 9.

The higher peak intensity of the 700 °C calcined sample as compared to the fresh one suggests that the crystallinity increased after the further calcination. Well crystallinity is essential for the high oxygen ionic conductivity, therefore, the 700 °C calcined sample was adopted for the further investigation and application.

The as-synthesized mixed powder of NiO and SDC was then soaked with 3N HNO_3 solution under heating. The NiO in NiO + SDC mixture was slowly dissolved and left behind a porous SDC powder. After the thoroughly washing and filtering, a pure-phase light-yellow SDC powder, as demonstrated by XRD examination, was obtained. The relative amount of nickel oxide applied in the synthesis was found to have significant effect on the properties of the SDC powder derived. For convenience, it is expressed as the weight ratio of NiO to SDC. Fig. 3 shows the XRD patterns of SDC samples after calcined at 700 °C for 3 h prepared with different amount of nickel oxide in the precursor. It indicates that all the powders displayed the typical fluorite phase structure, suggesting nickel did not cast negative effect on the phase formation. However, the diffraction peaks were gradually broadened with the increase of the NiO to SDC weight ratio, suggesting the decrease of the crystallite size of SDC. The calculated values were 13.7, 9.3 and 6.7 nm (showed in Table 1) at the NiO to SDC weight ratio of 0, 1 and 9, respectively. Therefore, nickel oxide actually acted an inhibitor for the crystallite size growth of the SDC powders. As shown in Table 1, the increase of NiO to SDC weight ratio also led to the increase of the surface area of the resulted SDC powder. A SDC powder with surface area as high as 77 $m^2\,g^{-1}$, crystalline size of ~6.7 nm and a pore volume of ~0.2276 $cm^3\,g^{-1}$ was obtained at the NiO to SDC weight ratio of 9. As a comparison, a surface area of only ~15 $m^2\,g^{-1}$ with the crystalline size of ~13.7 nm and a pore volume of ~0.1165 $cm^3\,g^{-1}$ was observed for the corresponding powder without the NiO templating.

Nitrogen adsorption/desorption isotherms and the corresponding BJH pore-size distribution curves (inset) of the as-synthesized SDC powders with different amount of NiO presence in the solid precursor are shown in Fig. 4. With respect to the IUPAC classification, the isotherms for the samples a and b are rather similar in shape to the type II isotherms, which show a weak narrow loop and exhibit an increase in total pore volume adsorbed near $p/p_0 = 1$. However, the samples a and b show some differences in BJH pore-size distribution (insert in Fig. 4a and b). The pore-size distribution of the sample a (as shown in the inset of Fig. 4a) shows nearly non-pore structure with a quite wide pore-size distribution. Compared with the sample a, the sample b (Fig. 4b) shows a relatively narrow pore-size distribution. Much different from the samples a and b, the sample c displays completely different isotherms and pore-size distribution. It shows IUPAC type IV isotherms with sharp inflection of nitrogen adsorbed volume at p/p_0 about 0.65, indicating the existence of mesopores. According to the isotherms, the pore-size distribution of sample c (inset in Fig. 4c) possesses mesopores with narrow pore-size distribution of mostly between 10 and 25 nm. Above results suggest that mesoporous SDC with high crystallinity and pore volume was able to be synthesized through the appropriate amount of in situ created NiO templating.

The morphologies of the SDC powders, prepared at NiO to SDC weight ratio of 0:1, 1:1 and 9:1, are shown in Fig. 5. The as-prepared SDC samples are in highly porous morphologic structure. The higher the NiO to SDC weight ratio the smaller the particle size was observed with a grain size of <100 nm for the sample prepared at the NiO/SDC weight ratio of 9. The highly porous structure of the powder together with the well nanocrystallinity is beneficial for a better performance electrocatalyst. The possible formation mechanism of the mesoporous SDC powders is shown in Fig. 6. At the NiO/SDC weight ratio of 1, the NiO particles primarily acted as an agglomeration inhibitor. The in situ created NiO particles broke up the three-dimensional network of SDC at a certain extent and inhibited the growth of the SDC particles. Therefore, an increase in surface area of SDC was observed with increasing the amount of nickel in the precursor. But quite a few NiO particles were also contained inside the SDC particles. After the dissolving of NiO by HNO_3 solution, pores were formed. As compared to that at other ratios, the inhibiting effect of NiO increased obviously at the condition of NiO to SDC weight ratio of 9. Under such situation, NiO also performed as an inorganic template for the formation of the mesoporous SDC. The NiO formed a network with the SDC clusters contained inside the NiO network. Some NiO par-

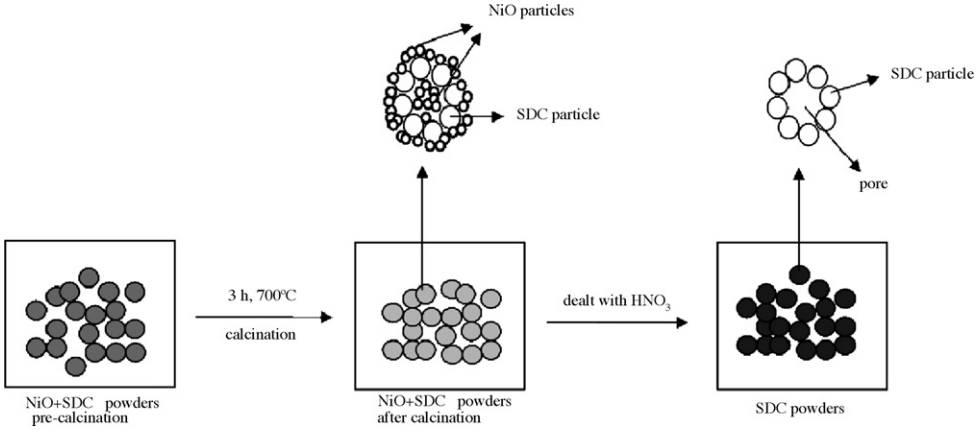

Fig. 6. Schematic diagram of possible formation processes of mesoporous SDC powder using in situ created NiO as template.

ticles were relatively uniformly dispersed in the SDC clusters. Mesopores were formed after wiped off the NiO particles from SDC.

The mesoporous SDC powder loaded with 7 wt.% Ru was then deposited onto the anode surface as the catalytic layer for the anode-supported SOFC. Fig. 7 shows the cross-sectional SEM micrographs of the MEA with the catalyst deposition after calcined at 700 °C for 2 h. The fuel cell was composed of four layers, the cathode layer with a thickness of 5–10 μm, the dense electrolyte layer with a thickness of ~30 μm, the anode SDC + NiO layer of ~500 μm, and the mesoporous SDC + Ru layer with a thickness of ~25 μm. The anode nickel was in nickel oxide state in Fig. 7. It shows that the catalytic layer was in highly porous state and attached to the anode layer really well.

Fig. 8a shows the typical voltage and power density versus current density of a SOFC based on thin-film SDC electrolyte (~30 μm) operated on 3% water humidified hydrogen at the flow rate of 90 mL min^{-1}, with a ~25 μm 7 wt.% Ru-loaded mesoporous SDC catalytic layer modified Ni + SDC anode and BSCF + SDC cathode. The fuel cell shows promising performance with a peak powder density of 850 and ~600 mW cm^{-2} at 650 and 600 °C, respectively. The high performance of the fuel cell at intermediate temperatures with hydrogen fuel was resulted from the high activity of the cathode for oxygen reduction [21] and the anode for hydrogen oxidation. Comparable performance was also observed for the similar fuel cell without the catalyst layer (as shown in Fig. 8b). It suggests that the catalytic layer did not cast significant negative effect on the fuel cell performance with hydrogen fuel. As pointed by Zhan and Barnett [10], the drawback of typical CeO_2–Ru catalyst layer laid on its reduction of the rate at which fuel can diffuse to the anode. Based on Fig. 7, the current Ru/SDC catalyst is in highly porous state, which ensures free gas transportation inside the catalytic layer. Furthermore, the pore size of 10–20 nm of the mesoporous SDC was about 25–60 times larger than the dynamic molecule radius of CO_2, H_2, CH_4, O_2 and CO molecules, which ensured the free gas diffusion inside the internal pores of SDC of the catalytic layer. The highly porous structure of the catalytic layer and the mesoporous structure of the compositional material of SDC then ensured the fast gas diffusion inside the Ru/SDC catalytic layer. Therefore, no such gas diffusion limiting of the fuel cell performance was observed even at high current density in the current Ru/SDC catalyst-modified fuel cells.

Fig. 9 shows the fuel cell performance with 3% H_2O humidified methane as the fuel at the flow rate of 30 mL min^{-1} for the fuel cells with or without the catalytic layer. An initial peak powder density of ~369 mW cm^{-2} were generated by the fuel cell without the catalytic layer, while a power density of ~462 mW cm^{-2} were yielded by the fuel cell with a porous Ru/SDC catalytic layer at 650 °C. The fuel cell with the Ru/SDC layer performed relatively stable, while the performance of the fuel cell without the catalytic layer deteriorated quickly. It is well known that methane has much worse electrochemical activity than H_2, especially at reduced temperature due to its much higher chemical stability. The promising fuel cell performance

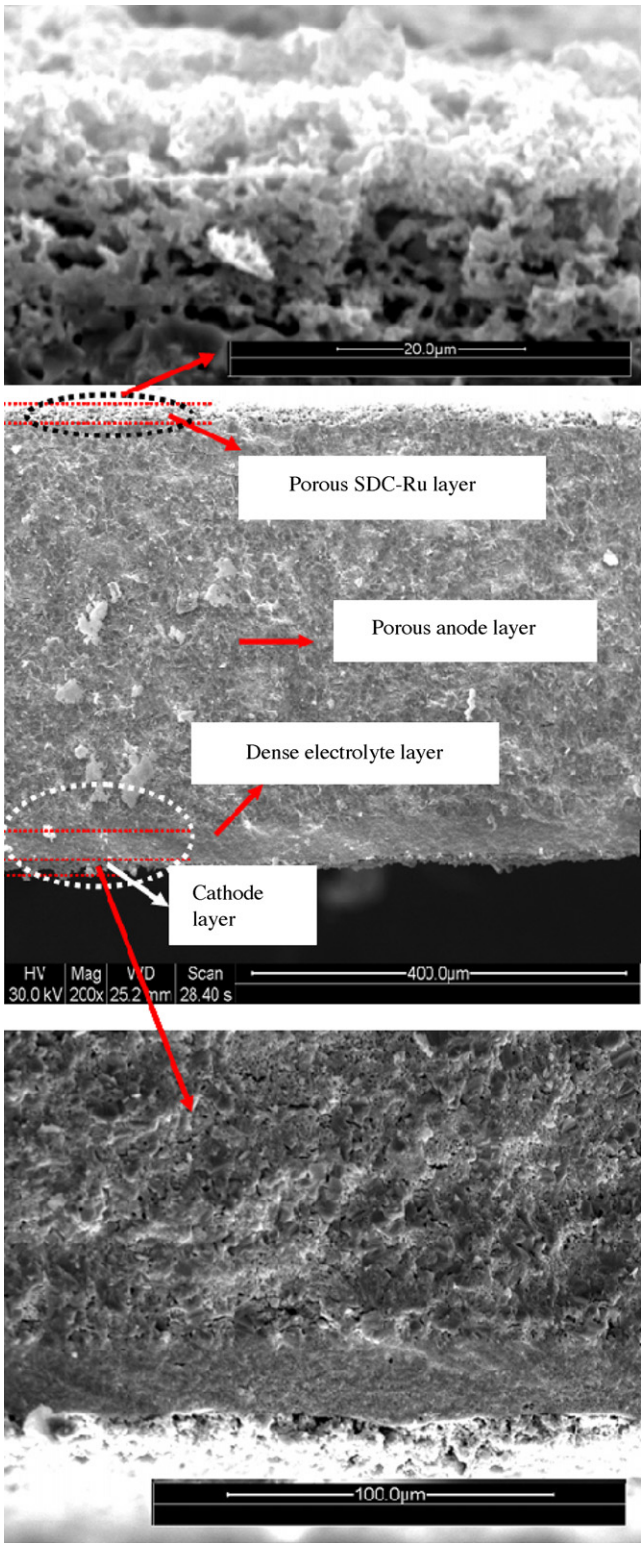

Fig. 7. SEM images of the typical anode-supported membrane electrolyte assemble (unreduced) with the porous SDC–Ru catalyst layer.

in current study was then attributed to the high activity of the Ru-loaded mesoporous SDC for methane electrocatalytical oxidation. As shown in Fig. 7, no observable agglomerated Ru grain was observed by SEM, suggesting that Ru was homogeneously distributed over the pore-wall of the mesoporous SDC. It then

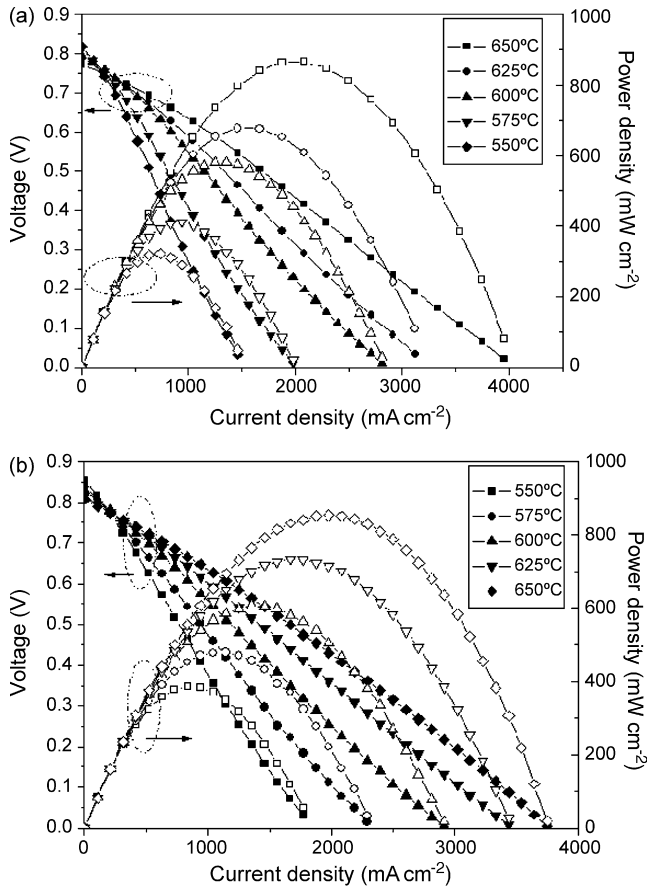

Fig. 8. Polarization curves for a cell using 3% H_2O humidified H_2 as fuel operated at various temperatures with (a) or without (b) a porous SDC–Ru catalyst layer.

ensured a large reaction area for methane oxidation. It is well known that Ru has high activity for water and CO_2 reforming of methane to syngas ($CO + H_2$) [22,23], while SDC or ceria favors the catalytic oxidation of methane to CO_2 and H_2O [1].

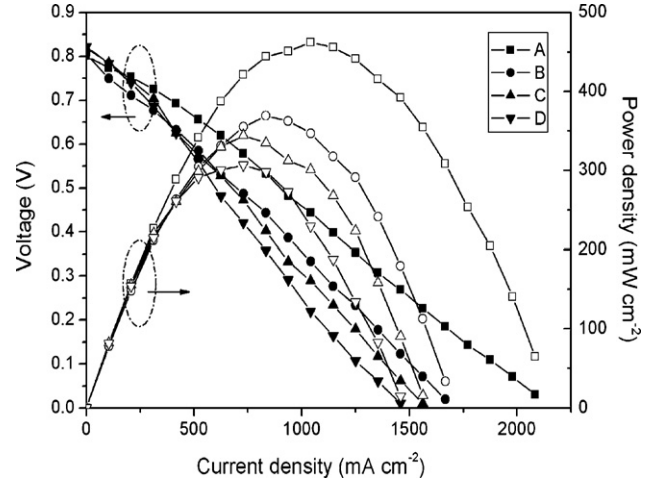

Fig. 9. Polarization curves for a cell using 3% H_2O humidified CH_4 as fuel operated at various temperatures with or without a porous SDC–Ru catalyst layer. A: C, D with a catalyst layer and at a temperature of 650, 625 and 600 °C, respectively and B: without the catalysts layer at 650 °C.

Therefore, in current methane-fueled SOFCs with Ru-loaded mesoporous SDC catalytic layer, it is likely that some methane was first oxidized to CO_2 and water under the electrocatalysis by the mesoporous SDC. Available additional methane was then internally reformed with the created water and CO_2 under the catalysis of Ru to form syngas ($CO + H_2$), which acted as the fuel for the following electrocatalytic oxidation. Since syngas has much higher electrochemical activity than methane, it then explained the observed favorable fuel cell performance even with methane fuel. Similar effect was also showed by Hibino et al. with the Ru–Ni–GDC anode. Furthermore, they achieved even higher performances as compared to the present results [23]. The detection of CO and H_2 species in the exhaust gas from the fuel cell by in situ gas chromatography supported the role of Ru in the internal reforming of methane to syngas. As we know, the carbon deposition may be a serious problem for the Ni-based anode directly operated on hydrocarbon fuels. After the tests, the fuel cells were conducted SEM examination. Some carbon coking was formed over the Ni + SDC anode surface for the fuel cell without the Ru/SDC layer, which well explained the quick deterioration of the fuel cell performance observed in this study. However, no observable carbon coking was formed over the anode surface of the catalyst-modified fuel cell.

We finally noted that the OCVs were relatively lower as shown in Figs. 8 and 9. One significant reason for this could be the internal shorting of the SDC electrolyte from its partial electronic conductivity [24]. Low OCVs were also reported by some other researchers with the anode-supported fuel cells based on doped ceria electrolyte [25–27]. Another possible reason is the mixed potential at the fuel cell cathode due to the gas leakage, which could be through the penetrated holes in the electrolyte layer or the silver sealant due to the imperfect sintering or sealing. Accordingly, the increment of the sintering temperature may eliminate the penetrated holes in electrolyte and be helpful to increase the OCV of the fuel cell. Indeed, we observed that when the sintering temperature of the electrolyte was elevated to 1450 °C, an OCV as high as 0.87 V or higher was observed at 600 °C.

4. Conclusion

In this work, mesoporous SDC powders with high surface area (77 $m^2\ g^{-1}$) were prepared via a facile glycine-nitrate combustion process with recyclable in situ created NiO as the inorganic template. The increase of relative amount of nickel nitrate in synthesis, resulted in the substantially change of the properties of the derived SDC powder, such as surface area, pore volume, and pore-size distribution. This method shows special advantages, such as easy to operate and reduction in capital cost, when comparing other synthesis techniques. It eliminates the application of expensive surfactants and organic templates. Furthermore, the inorganic template nickel applied in this study can be recycled after preparation. Acted as the catalytic layer, the mesoporous SDC displayed good performance for intermediate-temperature solid-oxide fuel cells with methane fuel.

Acknowledgements

This work was supported by the National Natural Science Foundation of China under contracts: No. 20646002 and No. 20676061. Dr. Zongping Shao also acknowledges the start-up funding from Nanjing University of Technology.

References

[1] S. Zhao, R.J. Gorte, Appl. Catal. A 277 (2004) 129.
[2] A. Yee, S.G. Morrison, H. Idriss, Catal. Today 63 (2000) 327.
[3] L.V. Mattos, F.B. Noronha, J. Catal. 233 (2005) 453.
[4] K. Otsuka, Y. Wang, M. Nakamura, Appl. Catal. A 183 (1999) 317.
[5] Z.P. Shao, S.M. Haile, J. Ahn, P.D. Ronney, Z.L. Zhan, S.A. Barnett, Nature 435 (2005) 795.
[6] S. Jung, C. Lu, H. He, K. Ahn, R.J. Gorte, J.M. Vohs, J. Power Sources 154 (2006) 42.
[7] S. Park, R. Cracium, J.M. Vohs, R.J. Gorte, J. Electrochem. Soc. 146 (1999) 3603.
[8] Z.P. Shao, J. Mederos, W.C. Chueh, S.M. Haile, J. Power Sources 162 (2006) 589.
[9] B.C.H. Steele, P.H. Middleton, R.A. Rudkin, Solid State Ionics 40/41 (1990) 388.
[10] Z.L. Zhan, S.A. Barnett, Science 308 (2005) 844.
[11] M. Antonietti, G.A. Ozin, Chem. Eur. J. 10 (2004) 28.
[12] M. Mamak, G.S. Metraux, S. Petrov, N. Coombs, G.A. Ozin, M.A. Green, J. Am. Chem. Soc. 125 (2003) 5161.
[13] B. Huang, X.F. Ye, S.R. Wang, H.W. Nie, R.Z. Liu, T.L. Wen, Mater. Res. Bull. (2006) doi:10.1016/j.materresbull.2006.11.027.
[14] C.W. Sun, Z. Xie, C.R. Xia, H. Li, L.Q. Chen, Electrochem. Commun. 8 (2006) 833.
[15] A. Martinez-Arias, M. Fernandez-Garcia, V. Ballesteros, L.N. Salamanca, J.C. Conesa, C. Otero, J. Soria, Langmuir 15 (1999) 4796.
[16] M. Lundberg, B. Skarman, L.R. Wallenberg, Microporous Mesoporous Mater. 69 (2004) 187.
[17] D. Terribile, A. Trovarelli, C.D. Leitenburg, G. Dolcetti, Chem. Mater. 9 (1997) 2676.
[18] D.M. Lyons, J.P. McGrath, M.A. Morris, J. Phys. Chem. B 107 (2003) 4607.
[19] W.H. Shen, X.P. Dong, Y.F. Zhu, H.R. Chen, J.L. Shi, Microporous Mesoporous Mater. 85 (2005) 157.
[20] W. Zhou, Z. Shao, W. Jin, J. Alloys Compd. 426 (2006) 368.
[21] Z.P. Shao, S.M. Haile, Nature 431 (2004) 170.
[22] A.T. Ashcroft, A.K. Cheetham, M.L.H. Green, P.D.F. Vernon, Nature 352 (1991) 225.
[23] T. Hibino, A. Hashimoto, M. Yano, M. Suzuki, M. Sano, Electrochim. Acta 48 (2003) 2531.
[24] C.R. Xia, W.L. Rauch, F.L. Chen, M.L. Liu, Solid State Ionics 149 (2002) 11.
[25] N. Ai, Z. Lü, K.F. Chen, X.Q. Huang, B. Wei, Y.H. Zhang, S.Y. Li, X.S. Xin, X.Q. Sha, W.H. Su, J. Power Sources 159 (2006) 637.
[26] Z.L. Zhan, S.A. Barrett, J. Power Sources 157 (2006) 422.
[27] A. Tomita, S. Teranishi, M. Nagao, T. Hibino, M. Sano, J. Electrochem. Soc. 153 (2006) 956.